ISSN 1392-3730/eISSN 1822-3605

VILNIUS TECH
Vilnius Gediminas Technical University

JOURNAL of CIVIL ENGINEERING and MANAGEMENT

2024
Volume 30
Issue 5
Pages 437–451
https://doi.org/10.3846/jcem.2024.21451

FRAGILITY ASSESSMENT OF INSTALLATION DEFECTS IN INDUSTRIAL STANDING SEAM METAL ROOF SUBJECTED TO WIND LOADS

Kyungrok KWON[1], Hyok Chu CHOI[2], Koochul JI[3], Youngjin CHOI[4], Jung Sik KONG[1]✉

[1] *Department of Civil, Environmental and Architectural Engineering, Korea University, Seoul 02841, Republic of Korea*
[2] *Global Loss Control Center, Samsung Fire & Marine Insurance Co., Ltd., Seoul 06626, Republic of Korea*
[3] *Korea Railroad Research Institute, Advanced Railroad Civil Engineering Division, South Korea, Seoul 02841, Republic of Korea*
[4] *Coastal Development and Ocean Energy Research Center, Korea Institute of Ocean Science and Technology, 385 Haeyang-ro, Yeongdo-gu, Busan, 49111, South Korea*

Article History:
- received 22 December 2022
- accepted 18 April 2024

Abstract. In industrial structures in which standing seam metal roofs (SSMRs) are commonly used, heat insulation and waterproofing have emerged as crucial requirements for the protection of internal equipment. However, in newly developed SSMRs, the structural systems have become increasingly complex. The installation of insulation layers between the upper and lower panels poses challenges during roof panel installations, resulting in defects owing to the carelessness of the installer. These clip defects can significantly affect the wind-resistance performance of the SSMR structure during testing. In this study, we employed finite element method (FEM) modeling and verification, utilizing the wind resistance test results of SSMRs. In addition, we conducted a variable analysis as well as a fragility assessment focusing on the location and number of clip defects in the SSMRs. The results of this study indicate that the wind performance of the roof was significantly degraded owing to SSMR clip defects. Moreover, the wind resistance performance can be quantitatively evaluated by considering the roof zone and the exposed environment under a wind load.

Keywords: industrial structures, fragility assessment, defected clips, FEM, SSMR, wind resistance.

✉Corresponding author. E-mail: *jskong@korea.ac.kr*

1. Introduction

Sandwich panels are used for construction in industrial buildings such as factories and logistics warehouses, offering advantages including convenient assembly, shortened construction time, and cost-effectiveness. Moreover, standing seam metal roof systems (SSMRSs) have been employed to shield expensive equipment from water damage and temperature fluctuations, with ongoing research in this area (Geng et al., 2021; Hoxha et al., 2022; Mohammadabadi et al., 2021). However, the wind resistance of recently installed SSMRSs has not been studied, with no research conducted on addressing the performance degradation owing to defects occurring during the installation process addressed in this study. Furthermore, owing to global warming, the climatic conditions in South Korea and other countries have transitioned to subtropical climates in recent years, which has led to an increased frequency of typhoons and the risk of strong winds, necessitating research on the safety of SSMRSs regarding wind resistance (Choi et al., 2017).

Strong winds, such as typhoons, can destroy sandwich panels in industrial structures. The destruction of these sandwich panels owing to these high winds results in expensive repair costs and damage to expensive equipment and stored products, leading to operational shutdowns in factories (Chowdhury et al., 2017; Konthesingha et al., 2015; Sivapathasundaram & Mahendran, 2018). To prevent damage, the aerodynamic characteristics acting on the roof panels must be understood. Azzi et al. (2020) conducted a wind tunnel experiment to study the impact of the shape and slope of a roof and wind direction on the average and standard deviation of the maximum wind pressure coefficient in open buildings, which provides realistic dynamic data. The conditions and mechanisms of the large local peak suction that occurs on roofs and walls

must be understood for the wind-resistant design of industrial structures. The peak suction of wind pressure is the most common cause of damage under strong wind conditions. When the wind is incident on the structure obliquely, peak suction occurs near the leading edge or corner of the roofs and walls (Mehta et al., 1992). Furthermore, predicting building damage caused by strong winds is essential for reducing economic losses.

Numerous studies have been conducted to mitigate the damage caused by strong winds in industrial buildings (Baskaran et al., 2012; Ji et al., 2022; Li & Stewart, 2011; Lu et al., 2022; Min et al., 2021; Pinelli et al., 2004; Wang et al., 2021). For instance, the wind resistance performance and failure patterns of metal-roof systems have been studied using finite element simulations. Moreover, the 360-degree locking joint has a wind resistance performance that is 3.24 times superior to that of existing roof systems (Lu et al., 2022). In addition, sliding supports connecting purlins to metal roofs have exhibited higher wind resistance and tensile strength than conventionally designed supports (Min et al., 2021). In this study, we assessed the structural wind resistance safety of SSMRs against uplift loads caused by winds based on wind resistance tests (Choi et al., 2021). Furthermore, based on the performance test results for the middle clip evaluated in this study, a finite element model was created, and using reinforced clips, the wind resistance performance was improved by 20.77% (Ji et al., 2022). However, these studies evaluated the wind resistance performance based on intact roof conditions. In recently used SSMRs, the prioritization of waterproofing and insulation functions has led to an increase in the height of the insulation material. Consequently, the installation process for SSMRs has become increasingly complex, resulting in defects in SSMR components owing to installation errors.

During wind resistance testing, defects were identified in clips that connect the roof panels and the saddle (Choi et al., 2021). These defects significantly contribute to the degradation of the structure's wind resistance performance. In this study, we aimed to understand the degradation of wind resistance performance owing to defects. The entire SSMR system was modeled using finite element analysis, and the results were compared with the static test results according to the ASTM E1592 international standard test method (ASTM International [ASTM], 2001). In addition, simple indoor experiments were conducted to assess the extent to which wind resistance performance decreased when defects occurred. Compared to previous studies, this study developed a method for predicting and evaluating the damage to SSMRs owing to construction defects when subjected to strong winds.

Analyzing the vulnerability of structures is an essential procedure required for performance-based design, which is the focus of recent design codes. For instance, it is crucial to predict the extent of damage, such as the probability of destruction, when unexpected events occur during the lifespan of a structure. Many researchers have developed extreme wind vulnerability models for various structures using reliability techniques (Gill et al., 2021; Lopez et al., 2020; Stewart et al., 2016; Zhang et al., 2021). However, these vulnerability assessment models have primarily been evaluated for residential buildings, such as single-family homes, and are not applicable to SSMRs, which are used to protect industrial structures. Moreover, research on the wind resistance performance of SSMRs regarding component defects is lacking. Therefore, SSMRs lack in terms of their structural performance, installation, and management capabilities.

The quality of structural components is crucial for the reliability of a structure's performance. However, the failure rate of components owing to human error is significantly high, in the range of approximately 75–90% (Brown & Yin, 1988; Madsen et al., 2006; Matousek, 1983; Stewart, 1993). Furthermore, quantifying installation errors caused by human mistakes is challenging. The current design codes for roof systems provide guidelines that do not consider component defects or material quality errors caused by installers, making them unreliable for structures such as SSMRS, which are prone to defects. Because of the characteristics of the SSMRS, monitoring the interiors of already-installed panels is challenging, which complicates the process of identifying the location and frequency of defects. A previous study could not detect whether a defect occurred in the mid-clip during the experiment until it was concluded, resulting in the degradation of the structural performance of the SSMR, as observed in the wind resistance test. Additionally, the experts and researchers conducting the experiments concluded that the occurrence of mid-clip defects among SSMRS components is crucial for determining the structure's performance. Therefore, industrial structures using the SSMR evaluated in this study may not perform as initially expected under strong winds in the case of defects in the roof, leading to potential destruction at wind speeds lower than the designed permissible wind speed.

In this study, we analyzed the structural performance of SSMRs based on engineering principles. Consequently, we developed a vulnerability model that can predict the damage to SSMRs exposed to strong winds, depending on the degree of component defects. Furthermore, a finite element model (FEM) subjected to static wind pressure was developed and analyzed based on the defect rate and location of the mid-clips. Simulations were conducted under various defect rates and locations to understand the wind resistance performance of the SSMR. Finally, we developed a vulnerability model considering the statistical characteristics of the wind resistance performance data and the variables required to calculate the wind load.

2. Clip-defect: defect resulting from an installer's lack of skill

During the installation of a structure, human or installation errors can cause structural defects. Quantifying these errors is complex because of the various reasons for failure, such as the installer's proficiency, location of the er-

ror, and number of errors within the structure (Nowak & Collins, 2012). The SSMR evaluated for wind resistance in this study was used to protect internal equipment within semiconductor production plant structures. Waterproofing and insulation are crucial for protecting temperature-sensitive semiconductor equipment. Therefore, the height of the insulation material increases, which complicates the installation process. Moreover, defects can occur in SSMR components owing to the installer's errors. These defects were determined by wind pressure tests (Choi et al., 2021; Hong & He, 2015), and the same type of SSMR was evaluated as has been used in this study. The wind resistance performance of the roof panel system for other types of standing seam metal panels varied depending on the defect condition of the component, even under the same testing conditions.

The test was conducted in accordance with ASTM E1592 standards (ASTM, 2001). The laboratory equipment used for the experiment included a fan capable of producing air flows of 2500 L/s and generating up to 10 kPa of wind pressure at a power of 37 kW. The required pressure levels for the experiment were realized by maintaining a constant fan speed and using a data logger to measure the displacement across the entire roof panel. The ASTM E1592 (ASTM, 2001) test involved the application of static pressure in constant increments to the underside of the specimen until the observation of major component failure. During this process, the panel's deflection and deformation were measured, yielding a load–deformation curve. In this study, the experiments were conducted with incremental loads of 0.5 kPa.

An examination of the type of damage incurred on the clip after the wind resistance test revealed a Y-shaped deformation, as shown in Figure 1a. However, in instances where installation errors occurred owing to worker oversight, the mid-clip may have developed an inward-bent portion during the fastening process. This resulted in an incomplete engagement with the panel, as shown in Figure 1b, thereby compromising the structural performance. Therefore, this study focused on the defects occurring in mid-clips to quantitatively evaluate the wind resistance performance of SSMRSs regarding defects arising during the SSMRS installation process.

Figure 2 shows an example of a wind pressure test with and without defects when the test was performed using the same method as in ASTM E1592 (ASTM, 2001). According to the graph, when a defect occurs in the mid-clip, it nearly reaches the point of failure at 4 kPa. In contrast, an intact roof panel displayed a stable performance up to 5.5 kPa. Because it is impossible to inspect the interior of already installed roof panels before the end of testing, it is challenging for managers and engineers to determine whether defects have occurred. Therefore, this study focuses on defects occurring in mid-clips during the installation process of the SSMRS, aiming to quantitatively evaluate the wind resistance performance of the SSMRS regarding these defects.

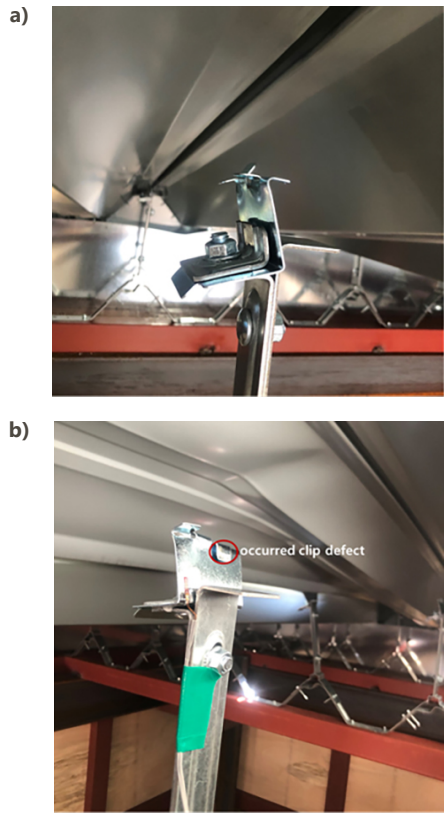

Figure 1. Failure shape of SSMR mid-clips: a – normal failure shape; b – failure shape when a defect occurs

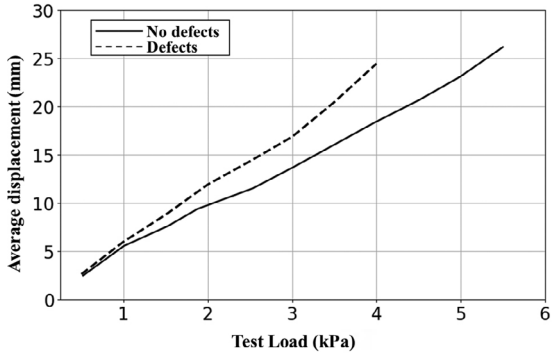

Figure 2. Comparison of wind test results of SSMRs with and without defects

2.1. Performance degradation owing to mid-clip defects

During the installation of the SSMRs, the mid-clips were coupled with the panels and then firmly fastened using specialized equipment. If the clips are not properly aligned and forced into position, defects can occur in the mid-clips. The occurrence of a small number of mid-clip defects does not significantly affect the wind-resistant performance of the structure. However, if a series of continuous defects occur along the line where the mid-clips are positioned, the clips fail to maintain their original wind-resistant performance. Therefore, to quantitatively evaluate the wind-resistant performance of mid-clips in the presence of defects, the structural performance affected by such defects

must be evaluated. Therefore, we compared the structural performance of the mid-clips in the presence or absence of defects through lab-scale experiments. The setup for the structural resistance experiment on the mid-clip and saddle was developed by the Korea Institute of Civil Engineering and Building Technology. As shown in Figure 3a (as a test method), a pull-out test was performed using a jig and fixing device, which was set up to secure the saddle universal testing machine (UTM). This method determines the stiffness of the components connecting the roof panels by measuring their displacement while increasing their load. Ji et al. (2022) described the detailed methodology of the test.

The clip used in the experiment had geometric dimensions of L 96/64 × H 63 × W 24 × T 1.0. Figure 3a shows the saddle and clip installed on the UTM machine. Additionally, as shown in Figure 3b, one of the clip parts was artificially induced to bend inward to simulate a defect for the experiment. Comparisons were made with cases where no defects occurred, and each test was performed three times. The measured load and displacement data were averaged and are listed in Table 1. The test revealed that when a defect occurred, the performance of the mid-clip was 30% lower than that of the mid-clip in the normal state. A 30% difference in performance before and after the occurrence of a defect in the mid-clip indicates that the failure rate of the entire SSMR system increases and its wind resistance system weakens as the number of defects in mid-clips continues to increase. Therefore, to evaluate the safety of facilities during strong winds quantitatively, assessing the reliability of the SSMR mid-clips based on the defect occurrence rate is crucial. Data samples for the reliability evaluation were secured through FEM, and the lab-scale data were used as spring property values for conducting evaluations according to the presence or absence of defects in the intermediate clip and saddle.

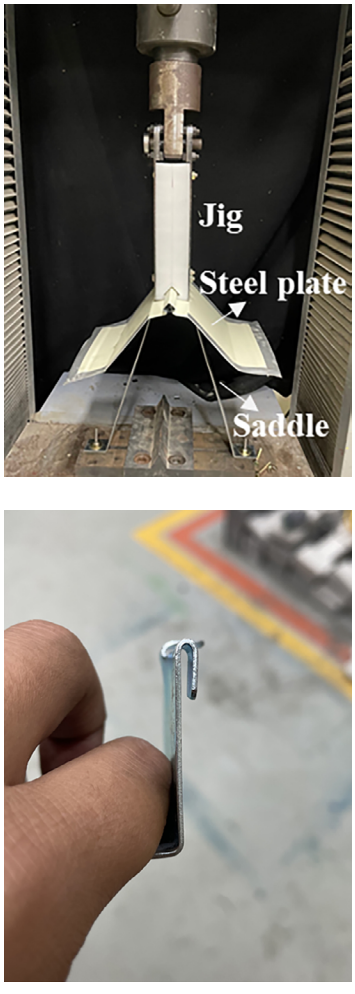

Figure 3. Experimental set-up of lab-scale test: a – exterior-interior; b – defect mid-clip

Table 1. Lab-scale test results

Mid-clip condition	Stiffness (kN/mm)	Yield displacement Δ (mm)
No defect	0.583	9
Defect	0.382	7

3. Numerical modeling

3.1. Verification of the analysis model

The induction of actual defects and the acquisition of data through static wind pressure experiments are suitable methods for assessing a structure's wind load performance based on the location and number of installation defects. However, these experiments are time-consuming and costly. Therefore, in this study, the finite-element program ABAQUS 2020 (ABAQUS, 2020) was used to predict the wind-load performance of the SSMR. The model developed in this study was validated by comparing the experimental results of an SSMR measured in a previous study. The parameters (W, L) used for the model's width (W) and total length (L) were W = 2925 mm and L = 5000 mm, respectively. For the roof panel components, the width, height, and thickness of the metal sheet were 650, 235, and 0.7 mm, respectively. In addition, the roof panel components, such as the saddle and clip, were the same as those used in the laboratory-scale tests. We used high-strength structural steel (SGC440 steel) for the roof panel. The material's characteristic values were set as: an elastic modulus of 200 GPa, Poisson's ratio of 0.3, and a yield strength of 375 MPa, as provided by the Korean Agency for Technology and Standards (2018).

Static analysis was conducted using the developed numerical model, and the results were compared with those obtained from the actual wind pressure test to validate the model. Figure 4 shows the information about the model employed to review the case study. The analysis model's load conditions were incrementally increased by 0.5 kPa, same as that in the internal wind resistance test conducted in previous studies. Vertical force was applied to the panel, increased in steps of 0.5 kPa for the analysis. In the actual wind pressure test, the edges of the panel and the base of the saddle were bolted to perform the wind load ex-

periment. Thus, the boundary conditions of the analysis model were fixed. Furthermore, the mid-clip connected to the panel was modeled using spring elements, and the boundary conditions at the base of the spring were also fixed. Defects were addressed by using springs for mid-clips, avoiding complexities arising from an increased number of meshes and the contact area between the panel and clip. Therefore, correctly modeling the clips with defects was crucial to examining the presence or absence of the defects addressed in this study. The challenges in validating the model for clips with and without defects as shell elements, as well as variable analysis, were mitigated by replacing the mid-clip with a spring. Laboratory-scale tests were employed to determine the properties of the mid-clips and saddles and model them as springs. The experimentally determined stiffnesses of defect-free and defective mid-clips were used to model the corresponding springs. A defective mid-clip had a 30% lower stiffness than that applied initially for the defect-free clip. The use of spring models facilitated variable analysis with simple tasks such as changes in stiffness. Spring models are used to depict the elastic connections between various components within a structure, including the links between roof panels and their supports. In this study, springs were employed to represent the constraints between mid-clips and roof panels. As a result, the modeled springs respond to the applied loads, exhibiting displacement values that correspond to the magnitude of these loads. For the simulation, 4-node reduced integral shell elements (Type S4R) were employed for both the end-clip and panel. The S4R element comprised four nodes, each providing three degrees of freedom for displacement and three for rotation. General contact conditions were applied for the end-clip's contact with the panel, whereas coupling conditions were used for the part where the mid-clip spring attaches to the panel.

To verify the analytical model, the average displacement measured in the wind pressure experiment was compared with the results of the FEM. Figure 5 shows the displacement measurement positions and comparison results. The displacement measurement positions were identical to those used in the wind pressure experiment. As shown in Figure 5b, the results of the static test and FEM simulation were similar. The FEM simulation results were lower than the static test results because the FEM simulation did not consider defects in the mid-clips. However, in the actual test, the mid-clip could possibly have defects that could potentially lower the wind resistance performance. Nevertheless, the error rate between the analytical model and the experimental results was within 10%. The method for calculating this error involved measuring the displacement with incremental increase in load by 0.5 kPa. Consequently, the error rate at these load increments was calculated and compared to assess the accuracy of the analytical model in simulating the structure's behavior under wind load conditions. In this study, variables were defined according to the occurrence rate and location of mid-clip defects using a verified analysis model, and case studies were conducted accordingly.

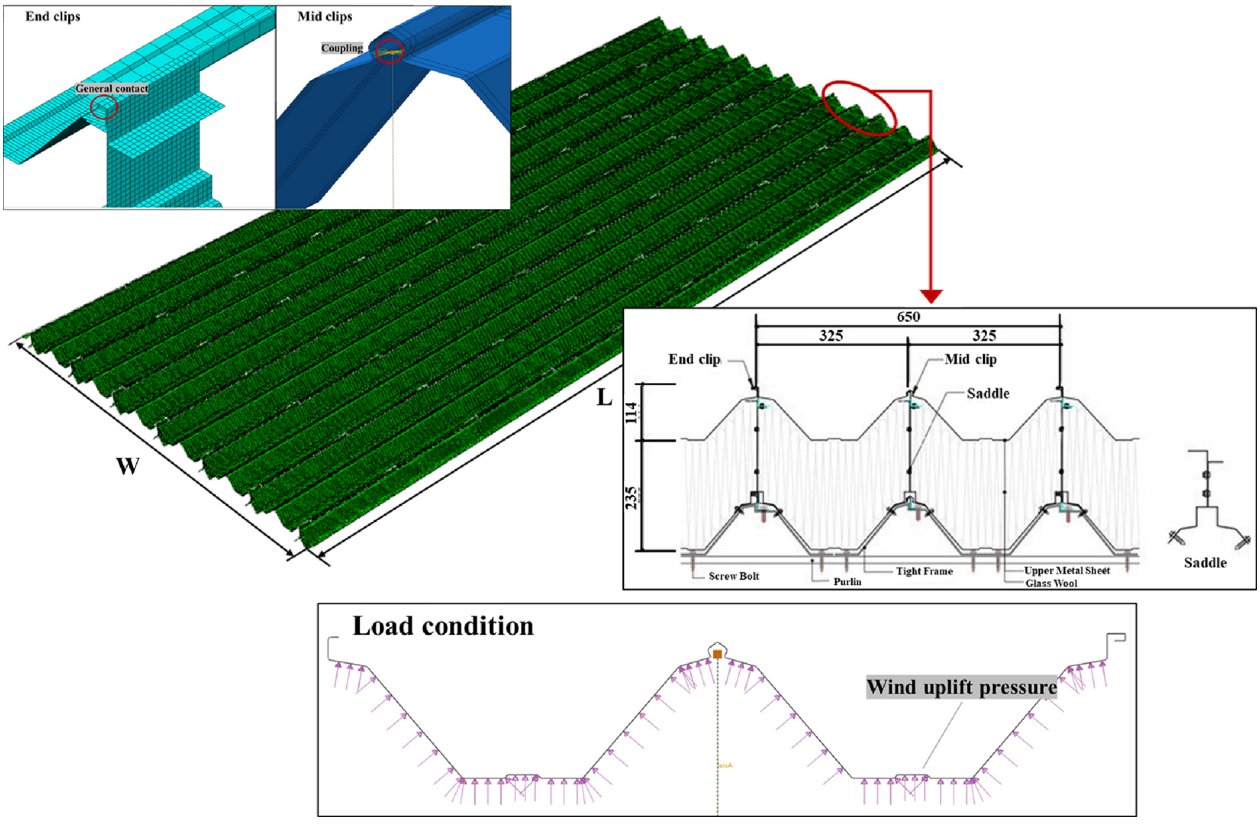

Figure 4. SSMR geometry information and FEM analysis details

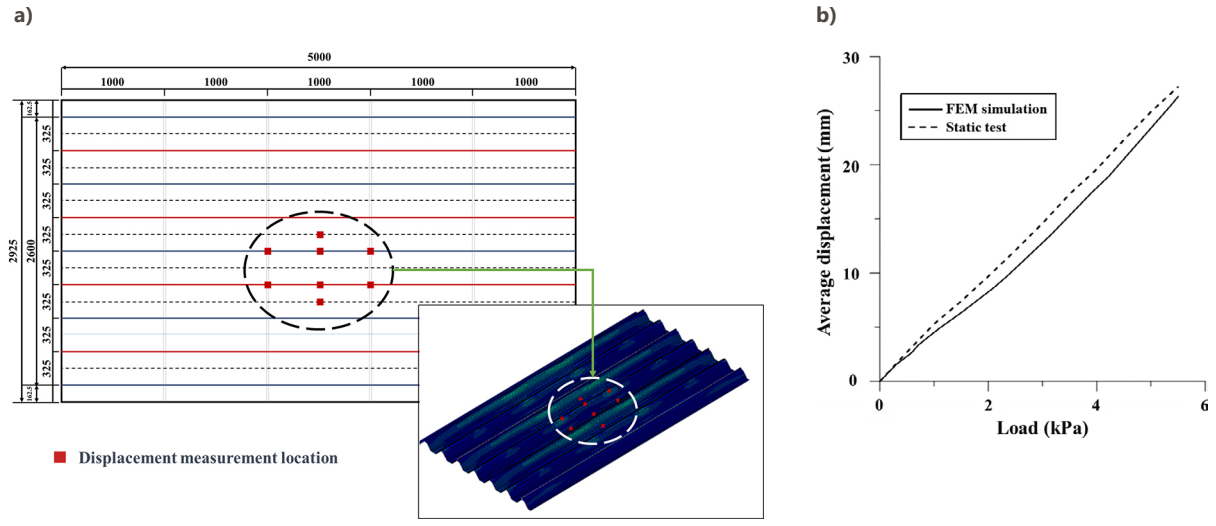

Figure 5. FEM results: a – location of the displacement measurements for the verification model (stress distribution); b – static wind resistance test results versus FEM simulation results

3.2. Results of the FEM simulation case study

To understand the wind resistance performance of an SSMR based on mid-clip defects that occur during its installation, the location and number of these defects must be identified. However, the panel interior is difficult to inspect once installed because insulating materials are inserted between the top and bottom sheets of the sandwich panel. Thus, in this study, we performed FEM analysis by designating the number and location of mid-clip defects as variables. For the various case studies, an FEM model with a width of 4230 mm and length of 1000 mm was constructed. The boundary conditions, loading conditions, and modeling methodologies were consistent with the analytical model used for validation. The model used in the case study consisted of 60 mid-clips and 60 end-clips. The destruction patterns observed after the wind pressure tests with defects were considered when determining the analytical cases. For example, based on the installation characteristics of the panels, a minimum of three consecutive defects are possible. For Set1 in Figure 6, defects (1), (2), (3), (4), (5) and (6) occurred consecutively. This also applied to the other cases. Furthermore, analyses were conducted on 37 sets to determine the structural performance based on the location of defects. For detailed information, please see Figure 6 and Table 2.

Thirty-seven FEM simulations were conducted to compare the wind resistance performance according to the mid-clip defect ratio. An example of an analysis in which no defects occurred is shown in Figure 7a. After the analysis, the displacement data were obtained at the nodes, as indicated in Figure 6. Subsequently, the average displacement at each location for a specific load was calculated. To determine the displacement values at specific loads, simple linear regression analysis was performed based on the measured data, as shown in Figure 7b. The α values obtained through regression analysis were used for vulnerability analysis, and the equation used for the regression analysis was $y = \alpha x$. When comparing the data with the regression equation, the coefficient of determination R^2 had a very high level of reliability, exceeding 0.9 in all cases.

The statistical properties obtained from these results were used in the vulnerability analysis. From Table 3, the alpha value increased as the mid-clip defect rate increased by 5%. Therefore, with increase in the defect occurrence, the critical roof displacement was reached more rapidly. For example, in the case of no defect, the alpha value was 4.62 mm/kPa; moreover, when the defect rate was 20%, the highest-risk alpha value was 6.69 mm/kPa. Thus, if the SSMR has a defect rate of 20%, the wind resistance performance can decrease by approximately 40% compared to that of the SSMR under normal conditions. Moreover, even with the same defect rate, the alpha value changed depending on the location of the defect. Thus, the location of defects can influence the vulnerability to wind resistance.

4. Fragility model for an SSMR subjected to a wind load

4.1. Fragility modeling

Structural fragility safety evaluation assesses the performance and reliability of structures constructed to withstand extreme conditions such as severe winds and earthquakes. When the load and resistance variables related to the limit state describing the strength and deformation are denoted by $X = X_1, X_2, X_3, ..., X_n$, the safety range of the structure can be defined using Eqn (1), as follows:

$$Z = g\left(X_1, X_2, X_3, \ldots, X_n\right) = R - S, \tag{1}$$

where $g(X)$ represents the function that describes the correlation between the applied load and resistance of the structure, R is the resistance, and S is the applied load on the structure.

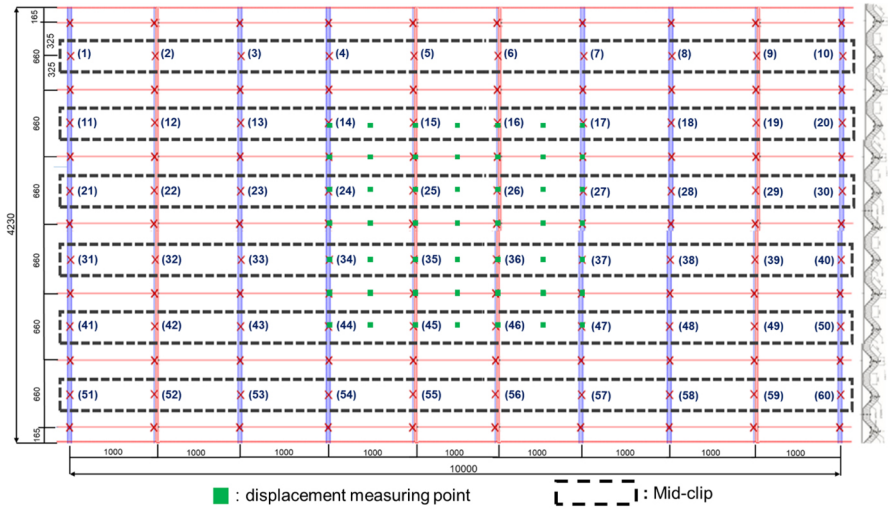

Set1	1,2,3,4,5,6	**Set10**	25,26,27,35,36,37	**Set19**	23,24,25,26,27,28, 45,46,47	**Set28**	1,2,3,4,5,6,7,8,9,,22, 23,24
Set2	2,3,4,5,6,7	**Set11**	25,26,27,45,46,47	**Set20**	23,24,25,26,27,28, 55,56,57	**Set29**	1,2,3,4,5,6,7,8,9,,24, 25,26
Set3	3,4,5,6,7,8	**Set12**	25,26,27,55,56,57	**Set21**	24,25,26,33,34,35, 36,37,38	**Set30**	3,4,5,6,7,8,23,24,25, 26,27,28
Set4	11,12,13,14,15,16	**Set13**	1,2,3,4,5,6,7,8,9	**Set22**	24,25,26,43,44,45, 46,47,48	**Set31**	13,14,15,16,17,18, 23,24,25,26,27,28
Set5	12,13,14,15,16,17	**Set14**	11,12,13,14,15,16, 17,18,19	**Set23**	24,25,26,53,54,55, 56,57,58	**Set32**	23,24,25,26,27,28, 33,34,35,36,37,38
Set6	13,14,15,16,17,18	**Set15**	21,22,23,24,25,26, 27,28	**Set24**	24,25,26,55,56,57, 58,59,60	**Set33**	23,24,25,26,27,28, 43,44,45,46,47,48
Set7	21,22,23,24,25,26	**Set16**	4,5,6,23,24,25,26, 27,28	**Set25**	1,2,3,4,5,6,7,8,9,12, 13,14	**Set34**	23,24,25,26,27,28, 53,54,55,56,57,58,
Set8	22,23,24,25,26,27	**Set17**	13,14,15,23,24,25, 26,27,28	**Set26**	1,2,3,4,5,6,7,8,9,13, 14,15	**Set35**	14,15,16,23,24,25, 26,27,28, 34,35,36
Set9	23,24,25,26,27,28	**Set18**	23,24,25,26,27,28, 34,35,36	**Set27**	1,2,3,4,5,6,7,8,9,16, 17,18	**Set36**	14,15,16,23,24,25, 26,27,28,44,45,46

Figure 6. FEM displacement measurement location and SET (mid-clips defect case) information

Table 2. Case details and defect location based on the defect rate

Mid-clip defect ratio (%)	Defect location	Case
0	–	1
10	Set1, Set2, Set3, Set4, Set5, Set6, Set7, Set8,Set9, Set10, Set11, Set12	12
15	Set13, Set14, Set15, Set16, Set17, Set18, Set19, Set20, Set21, Set22, Set23, Set24	12
20	Set25, Set26, Set27, Set28, Set29, Set30, Set31, Set32, Set33, Set34, Set35, Set36	12

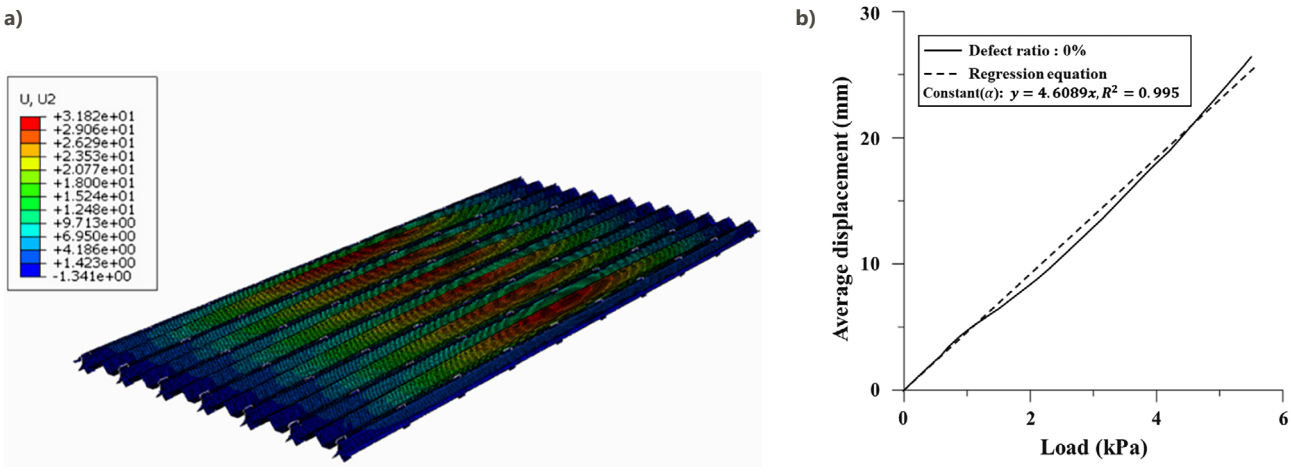

Figure 7. FEM simulation results for a 0% defect rate: a – numerically predicted Y-axis displacements; b – load/displacement curve versus linear regression equation

Table 3. Results of FEM simulation for constant α

Mid-clip defect ratio: 10%				Mid-clip defect ratio: 15%				Mid-clip defect ratio: 20%			
Set	α (mm/kPa)	Mean	Standard deviation	Set	α (mm/kPa)	Mean	Standard deviation	Set	α (mm/kPa)	Mean	Standard deviation
Set1	5.22	5.51	0.18	Set13	5.69	5.91	0.12	Set25	6.21	6.47	0.14
Set2	5.24			Set14	5.71			Set26	6.22		
Set3	5.29			Set15	5.86			Set27	6.29		
Set4	5.51			Set16	5.83			Set28	6.38		
Set5	5.55			Set17	5.93			Set29	6.42		
Set6	5.54			Set18	6.01			Set30	6.43		
Set7	5.62			Set19	5.96			Set31	6.55		
Set8	5.65			Set20	5.87			Set32	6.65		
Set9	5.79			Set21	6.12			Set33	6.51		
Set10	5.42			Set22	6.01			Set34	6.47		
Set11	5.77			Set23	5.99			Set35	6.69		
Set12	5.47			Set24	5.97			Set36	6.58		

Note: Mid-clip defect ratio: 0%; α (mm/kPa): 4.62 (deterministic).

Vulnerability can be defined as the conditional probability of the functional failure of structural components or systems for a given set of input variables. Vulnerability is expressed as follows, using Eqn (2):

$$P_f = P\left(Z < 0\right) = \Sigma\left[Z\left\langle 0 \middle| D = x\right]P\left[D = x\right], \tag{2}$$

where D denotes a random demand on the load, $Z < 0$ represents the limit state, and $\left[Z\left\langle 0 \middle| D = x\right]\right.$ denotes the conditional limit state probability given a certain D. Eqn (2) can also be expressed in convolutional integral form if the demand x is a continuous function of the hazard, as shown in Eqn (3) (Melchers & Beck, 2018):

$$P_f = P\left(Z < 0\right) = \int_0^\infty F_r\left(x\right)G_x\left(x\right)d_x, \tag{3}$$

where $F_r(x)$ denotes the fragility function of demand x expressed in the form of a cumulative distribution function, and $G_x(x)$ represents a hazard function expressed in the form of a probability density function. The fragility $F_r(x)$ of a structural system can be modeled using a lognormal distribution and is expressed using Eqn (4), as follows (Kennedy & Ravindra, 1984; Masanobu et al., 2000; Straub & Der Kiureghian, 2008):

$$F_r\left(x\right) = \Phi\left[\frac{\ln\left(x\right) - \lambda_R}{\xi_R}\right], \tag{4}$$

where Φ[·] denotes the standard normal cumulative distribution function (often referred to as the Gaussian), λR denotes the median capacity of R, ξ denotes the standard deviation of natural logarithm. The vulnerability of a structure can be determined through a probabilistic analysis of several variables. Vulnerability can be used to identify the level of demand that a component or system can tolerate with a particular probability. Fragility curves provide engineers with condition assessments and design applications (Ellingwood et al., 2004).

In this study, the concept of fragility was applied to perform a wind fragility analysis of SSMR, and a limit state equation was formulated for this purpose. The destruction of the SSMR was assumed to occur because of wind loads. The limit state equation for the wind loads on the SSMR is expressed as follows:

$$Gx\left(R, Z\right) = R - Z, \tag{5}$$

where R denotes the wind load resistance capacity probability distribution of the SSMRS (statistical values of roof panel failure displacement during wind resistance tests) and Z denotes the displacement probability distribution during the action of a wind load on the SSMRS.

A detailed explanation of the variables for the limit state used in this study is provided in Sections 4.2 and 4.3. Furthermore, to analyze the degradation of wind-resistance performance in the case of mid-clip defects, defect rates of 0, 10, 15, and 20% were defined for the vulnerability analysis. Thus, the failure probability can be calculated using the limit state of the mid-clip defect rates in the SSMR during strong winds. Additionally, by employing Eqn (4), vulnerability curves based on defect rates and wind speeds can be obtained.

4.2. Limit state function resistance capacity statistics of an SSMRS

The statistical characteristics of resistance performance (R) used in this study are based on actual wind pressure test results. The average displacement data for which the panel was destroyed when subjected to wind resistance pressure on the SSMRS was assumed to follow a normal distribution. The total sample size was four. The population mean and coefficient of variation of the displacement measured when a wind load was applied to the SSMR are listed in Table 4. The use of only four data points to determine the statistical characteristics of resistance performance may

be insufficient. However, these distribution characteristics were determined by referencing the statistical values of the resistance performance from previous studies related to domestic standing seam metal roofs (Lee & Rosowsky, 2005; Lee et al., 2013). The limited sample size of four in this study, while a constraint, is consistent with common practices in structural engineering research, wherein extensive data collection is often challenging. This approach is supported by the patterns observed in our data, which are consistent with findings in related literature, such as the study by Lee and Rosowsky (2005). Future research with larger sample sizes and more diverse data is recommended to further validate and enhance the understanding of SSMR's wind resistance characteristics.

Table 4. Statistics of the resistance performance of the SSMRS

No.	Failure average displacements (mm)	Probability distribution	Mean & Standard deviation
1	28	Normal	Mean: 28.5 mm Standard deviation: 1.41
2	30		
3	29.5		
4	26.4		

The average displacement at failure of the resistance performance (R) used in this study was 28.5 mm, with a standard deviation of 1.41. The failure displacement was determined by averaging the displacements measured at various locations when the SSMR was destroyed during the static wind resistance experiment. Furthermore, the averages and standard deviations of the measured failure displacements for each experiment were used as the resistance performance measures in the SSMR limit-state equation.

4.3. Statistics for wind load effects

To evaluate the fragility of an SSMR in the limit state, the response of the structure to the load must be defined. In this study, the displacement response of the structure to the load was utilized. The equation below is adapted from the ASCE 7-10 (American Society of Civil Engineers [ASCE], 2010), ASCE 7-16 (ASCE, 2016), and Korean Building Code (Architectural Institute of Korea, 2016) equations that determine the uplift pressure caused by wind loads. In this study, a modification was made to the traditional wind load calculation by introducing a constant 'α'. This modified Eqn (6) allows the estimation of the displacement that can occur under a particular load:

$$Z = \alpha q_h \left[GC_p - GC_{pi} \right] \text{ (units: mm)}, \quad (6)$$

where α denotes the constant that converts the wind load acting on the roof panel into a displacement constant (units: mm/kPa), q_h denotes the velocity pressure evaluated at the mean roof height h (units: kPa), GC_p denotes the external pressure coefficient, and GC_{pi} refers to the internal pressure coefficient.

The wind pressure was varied to vary the displacement value because the resistance performance (R) of the limit state equation used in this study was also evaluated based on the displacement. To calculate the response to the load, the velocity pressure at a certain height must be calculated as follows:

$$q_h = 0.613 K_z K_{zt} K_d V^2 I \text{ (units: N/m}^2\text{)}, \quad (7)$$

where q_n is equivalent to q_h at the mean roof height; K_z is the velocity pressure exposure factor; K_{zt} is the topographic factor; K_d is the wind direction factor; V is the basic wind speed; and I is a crucial factor. Moreover, the wind is subject to numerous variations.

In this study, we referenced previous studies to consider the variability in the calculated wind pressure (Chauhan et al., 2022; Ellingwood & Tekie, 1999; Lee & Rosowsky, 2005; Lee et al., 2013). The statistics must be obtained based on location and building information from a factory site. However, such data are currently insufficient in Korea. Although in domestic research, assuming that all wind statistics follow a normal distribution is unreasonable, a normal distribution is used for the statistics required when calculating various wind loads (Lee et al., 2013). Therefore, we assumed a normal distribution and conducted a vulnerability analysis. In the future, by building and analyzing the data on the variables required for wind load calculation, we will be able to identify the statistical characteristics and improve the accuracy and reliability of our research results. Table 5 shows the statistical characteristics of the variables used in previous studies, and Figure 8 illustrates the roof zones as defined in the design standards.

Table 5. Summary of wind load statistics

Parameters	Description	Mean	Standard deviation	CDF
K_z	ExpB (0.0 m–9.1 m)	0.71	0.19	Normal
	ExpC (0.0 m–6.1 m)	0.84	0.14	
	ExpD (0.0 m–4.6 m)	0.99	0.14	
K_d	Components and cladding	0.89	0.16	Normal
GC_{pi}	Enclosed	0.15	0.33	Normal
	Partially enclosed	0.46	0.33	
GC_p	Zone 1	–1.41	0.22	Normal
	Zone 2	–2.34	0.22	
	Zone 3	–3.23	0.22	
K_{zt} I	1.0 (deterministic)			

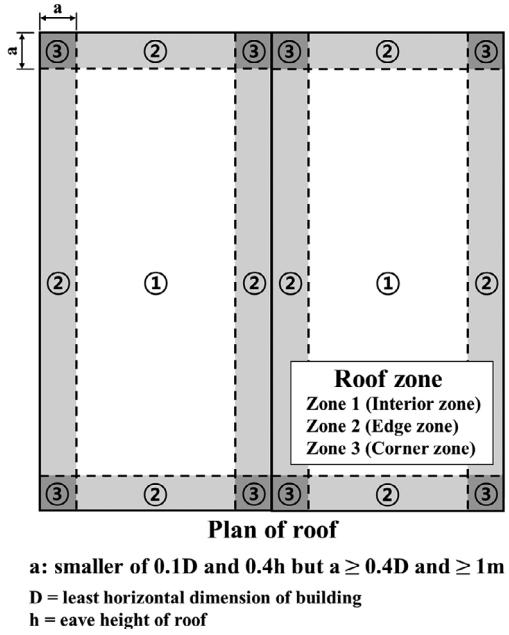

Figure 8. ASCE 7-10 and KBC 2016 wind pressure zones on roof (h ≤ 60 ft)

5. Results of fragility assessment

Fragility assessment of the structure was conducted based on the variability of various parameters. The reliability analysis was divided into sampling-based and data-analysis methods and employed to address these uncertainties. Sampling-based methods such as Monte Carlo simulations require numerous samples to ensure the reliability of the results. Therefore, in this study, the first-order reliability method (FORM) was used to calculate the failure probability of the SSMR. FORM is a probabilistic analysis method used to estimate the reliability of complex engineering systems. This method simplifies the calculation process by linearizing the limit state function at the point of highest failure probability, thus approximating the failure probability. The main assumptions of FORM include the normality of the base variables and linearity of the limit state function in the transformed space. It calculates the failure probability by determining the shortest distance from the origin to failure surface in the space of standard normal distribution variables, known as the reliability index (Baran, 2023; Du & Hu, 2012; Maier et al., 2001). However, the reliance on the normality assumption and linear approximation can reduce the accuracy, especially for systems with nonlinear behavior or non-normal distributions. Despite this issue, FORM is widely used in structural reliability analysis because it simplifies complex reliability problems, allowing for efficient processing and meaningful results at lower costs. Figure 9 illustrates the principles and procedures of FORM. We estimated the failure probability using Eqns (5) and (6); however, Eqn (4) allowed us to calculate the parameters required for drafting the vulnerability curve.

In the developed FEM, the simulation considered factors such as the presence or absence of defects in the mid-clip and their location. Furthermore, the failure probability for a specific wind speed was calculated using displacement data. Additionally, a reliability analysis was performed considering related variables, such as the exposure conditions based on the ground roughness, allowing for an efficient evaluation of the wind resistance vulnerability of the SSMR.

The wind-speed-related destruction probabilities calculated under various conditions are listed in Table 6. Figure 10 shows the vulnerability curves for the three roof zone conditions under the 20% exposure environment D. When a strong wind, similar to a typhoon of approximately 40 m/s, blows, the failure probabilities for Zones 1, 2, and 3 are 0.21, 13, and 55.8%, respectively. Therefore, Zone 3 must be prioritized in preparation for strong winds. In Figure 11, we observe a decrease in the initial wind speeds that cause damage to the SSMR as we move away from exposure categories B to D. Exposure to Environment D, owing to its coastal area characteristics, poses a higher risk, necessitating additional attention and preparedness. Figure 12 shows that installation defects in the intermediate clips significantly impact the wind vulnerability of the SSMR. For instance, in exposure category D (zone 3), when the wind speed reached 30 m/s, the failure probability was 0% for a defect rate of 0%. However, if the defect rate is between 10% and 20%, the SSMR can be damaged at wind speeds of 30 m/s. Additionally, the buildings in some coastal regions of Korea have been designed for wind speeds of 40 m/s. Therefore, buildings in these regions can be damaged with a high probability at wind speeds lower than the intended design strength.

5.1. Wind resistance safety evaluation of SSMRs using fragility curves

To understand the vulnerability assessment process of the SSMR developed in this study, a wind-resistance evaluation was conducted using an actual basic wind-speed map for South Korea. Figure 13 shows a basic wind speed map developed using the wind speed data provided by the Korea Meteorological Administration and the design wind speed supplied by the Korean Building Code (Architectural Institute of Korea, 2016; Jeong et al., 2014). The proximity to the sea in Korea increases the impact of strong winds, such as typhoons. The structures constructed along the coastline experience a greater vulnerability to strong winds, especially industrial buildings that use SSMRs. Therefore, the evaluation target of this study was a factory located in Busan. Using the basic wind speed map and the design wind speed from the Korean Building Code, the wind speed range was set at 35 to 40 m/s. The exposure category of industrial structures built near the coast used for evaluation was ExpD. However, the mid-clip defect rate of warehouses was 10%. Under these eval-

Table 6. Failure probabilities obtained from FORM

Defect ratio	Exp	Zone	Wind speed (m/s)				
			30	40	50	60	70
0	B	Zone 1	0	0	0	7.18.E–03	7.47.E–02
		Zone 2	0	0	2.75.E–02	2.52.E–01	5.99.E–01
		Zone 3	0	1.59.E–02	2.93.E–01	7.06.E–01	9.04.E–01
	C	Zone 1	0	0	0	1.24.E–02	1.30.E–01
		Zone 2	0	1.03.E–02	5.11.E–02	4.24.E–01	7.15.E–01
		Zone 3	0	2.90.E–02	5.10.E–01	8.09.E–01	9.27.E–01
	D	Zone 1	0	0	0	4.42.E–02	2.77.E–01
		Zone 2	0	1.41.E–02	1.55.E–01	6.65.E–01	9.34.E–01
		Zone 3	0	1.07.E–01	6.33.E–01	8.72.E–01	9.59.E–01
10	B	Zone 1	0	0	1.08.E–03	4.25.E–02	2.06.E–01
		Zone 2	0	1.90.E–02	1.78.E–01	4.63.E–01	7.02.E–01
		Zone 3	0	1.31.E–01	5.01.E–01	7.68.E–01	9.17.E–01
	C	Zone 1	0	0	1.91.E–02	1.35.E–01	3.59.E–01
		Zone 2	0	3.38.E–02	2.77.E–01	6.12.E–01	8.22.E–01
		Zone 3	0	2.42.E–01	6.52.E–01	8.70.E–01	9.48.E–01
	D	Zone 1	0	0	3.81.E–02	2.37.E–01	5.03.E–01
		Zone 2	0	7.25.E–02	4.26.E–01	7.42.E–01	9.52.E–01
		Zone 3	1.81.E–02	3.89.E–01	7.74.E–01	9.22.E–01	9.68.E–01
15	B	Zone 1	0	0	7.58.E–03	7.93.E–02	2.68.E–01
		Zone 2	0	1.37.E–02	1.86.E–01	5.26.E–01	7.86.E–01
		Zone 3	2.33.E–03	1.54.E–01	5.72.E–01	8.49.E–01	9.52.E–01
	C	Zone 1	0	0	1.36.E–02	1.35.E–01	4.04.E–01
		Zone 2	0	3.98.E–02	3.05.E–01	7.11.E–01	9.16.E–01
		Zone 3	4.02.E–03	2.60.E–01	7.58.E–01	9.53.E–01	1.00.E+00
	D	Zone 1	0	0	4.00.E–02	2.56.E–01	5.77.E–01
		Zone 2	0	9.19.E–02	4.93.E–01	8.50.E–01	9.67.E–01
		Zone 3	2.31.E–02	4.47.E–01	8.83.E–01	9.84.E–01	1.00.E+00
20	B	Zone 1	0	0	1.00.E–02	1.04.E–01	3.34.E–01
		Zone 2	0	1.81.E–02	2.41.E–01	6.24.E–01	8.64.E–01
		Zone 3	2.97.E–03	2.02.E–01	6.72.E–01	9.15.E–01	9.81.E–01
	C	Zone 1	0	4.42.E–04	2.93.E–02	2.04.E–01	4.99.E–01
		Zone 2	1.24.E–04	5.26.E–02	4.09.E–01	7.83.E–01	9.41.E–01
		Zone 3	1.18.E–02	3.64.E–01	8.23.E–01	9.67.E–01	1.00.E+00
	D	Zone 1	0	2.09.E–03	6.47.E–02	3.48.E–01	6.64.E–01
		Zone 2	7.82.E–04	1.30.E–01	5.98.E–01	8.93.E–01	9.77.E–01
		Zone 3	4.02.E–02	5.58.E–01	9.18.E–01	9.88.E–01	1.00.E+00

uation conditions, the calculated probability of destruction can be represented as a vulnerability curve shown in Figure 14 and can be calculated through the log-normal distribution parameters shown in Eqn (4). The optimal log-normal parameters derived from the calculated probability of destruction are as follows: (Zone 1: λR: 4.2419, ξR: 0.1817), (Zone 2: λR: 3.9596, ξR: 0.1843), (Zone 3: λR: 3.7761, ξR: 0.2191).

Upon evaluating the wind resistance safety of a factory located in Busan, considering the mid-clip vulnerability curve of SSMR, we found that Zones 1 and 2 have a low damage probability of less than 10%. However, Zone 3 exhibited a high failure probability of 38.9% at a wind speed of 40 m/s. Therefore, factory managers should prioritize reinforcing Zone 3 before the onset of typhoons or strong winds to prevent potential damages. As a method of reinforcement, using wind clips on the SSMR can be effective. According to a study by Ji et al. (2022), reinforcing the mid-clip results in a 20.77% enhancement in strength. By employing such methods, factory managers and designers can proactively identify vulnerable locations and prevent accidents before the occurrence of strong winds.

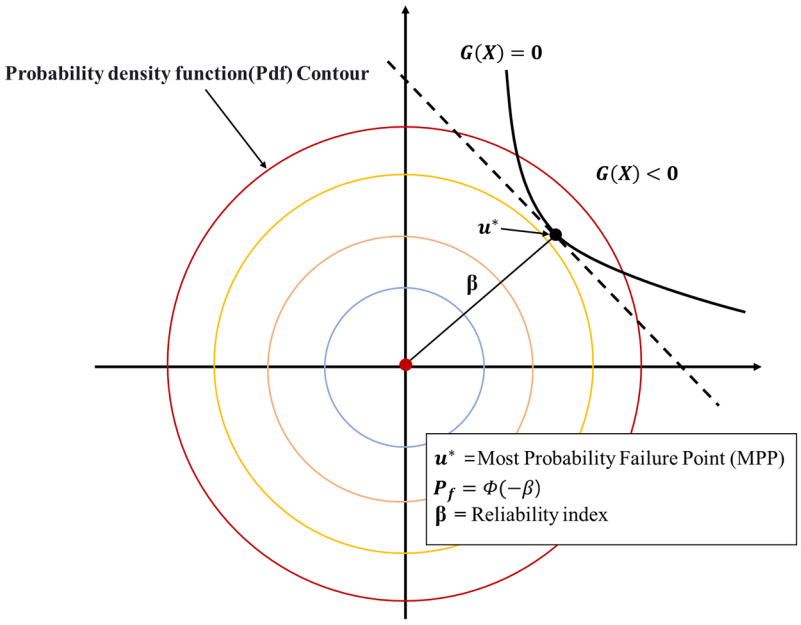

Step 1: Define the limit state function, which represents the threshold between the safe and failed states of the system

Step 2: Transform the original variables into standardized normal variables to simplify the limit state function.

Step 3: Linearize the limit state function around the design point, which is the most probable point of failure on the limit state surface in the transformed space.

Step 4: Determine the reliability index (β), which is the shortest distance from the origin to the linearized limit state function in the standard normal space.

Figure 9. Basic idea of FORM

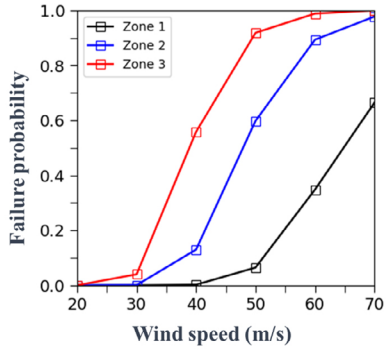

Figure 10. SSMRS fragility for three roof zones [defect ratio 20%, ExpD]

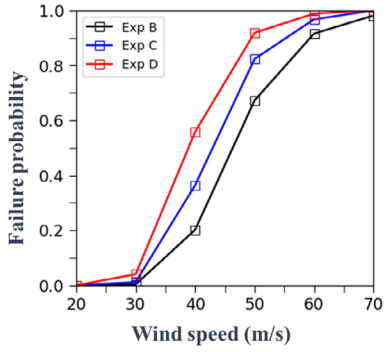

Figure 11. SSMR fragility for different exposure categories [defect rate 20%, zone 3]

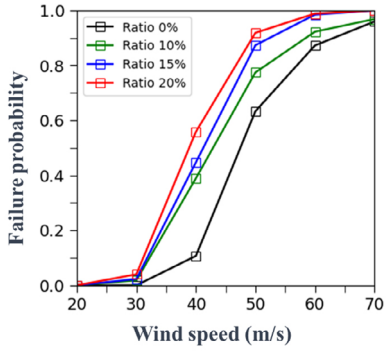

Figure 12. SSMRS fragility of mid-clip defect rate [ExpD, zone 3]

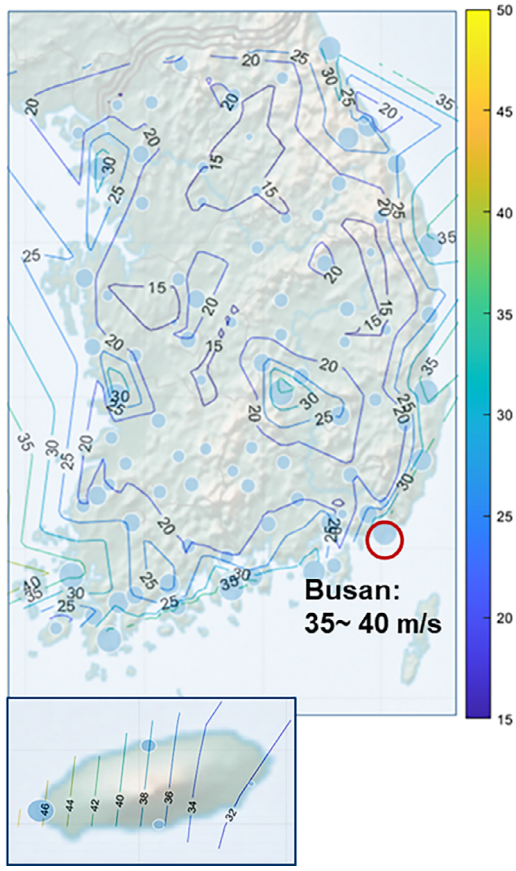

Figure 13. Wind basic map in South Korea

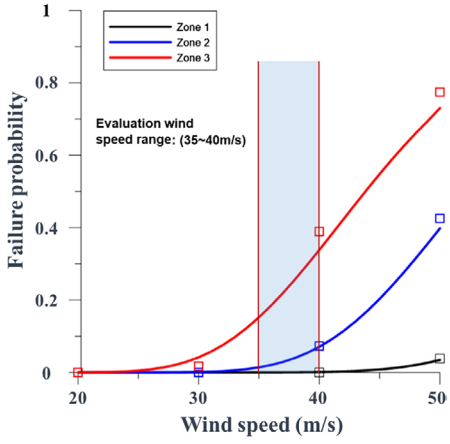

Figure 14. Evaluating wind resistance of SSMRs using fragility curves (Busan, 10% defect rate, ExpD)

6. Conclusions

Based on various simulation and experimental results, this study assessed the vulnerability of SSMR to extreme wind conditions. Additionally, it provided information about potential defects that could arise during the construction phase, and clarified the performance degradation of structures due to these defects. The primary outcomes obtained from this analysis are as follows:

(1) Due to its intricate system characteristics, various defects can arise during the installation of the SSMR. A notable defect observed was the damage to the mid-clip during the installation process. In this study, we confirmed approximately a 30% strength reduction through indoor experiments when this clip defect occurred. Based on these experimental results, we developed an analytical model to evaluate the wind resistance performance of SSMR considering these defects.

(2) Predicting the rate and location of defects during the installation process of SSMR is challenging. Therefore, in this study, we set up 37 cases and performed finite element analysis. The results demonstrated significant performance variations in the overall structural system, even with the same defect, depending on its occurrence location and frequency.

(3) This research analyzed the vulnerability based on the mid-clip defect using the analysis results and wind pressure experiment data. The vulnerability analysis utilized the FROM analysis, revealing that under wind speeds of 40 m/s, there was approximately a fivefold increase in destruction probability based on the defect rate. Furthermore, we were able to draft a vulnerability curve, which can be employed to estimate damage costs and devise preventive strategies.

This methodology is applicable not only in South Korea but also internationally for designing industrial structures. Engineers can utilize these probabilistic design data by considering factors such as exposure surface roughness, contemplated defect rate, and design wind speed. Methods for adjusting safety rates based on the importance of industrial structures have been developed. However, more research incorporating uncertainties based on the actual plant and environmental data is required to derive more detailed research outcomes using analytical and experimental data.

Acknowledgements

This work supported by the Korea Railroad Research Institute (KRRI) (PK2403A2) and National Research Foundation of Korea (NRF) grant funded by the Korea government (MSIT) (No. RS-2024-00346542).

Author contributions

Conceptualization, Kyungrok Kwon and Jung-Sik Kong; methodology, Koochul Ji and Hyok Chu Choi; validation, Kyungrok Kwon, Hyok Chu Choi, and Koochul Ji; formal analysis, Kyungrok Kwon and Koochul Ji; investigation, Hyok Chu Choi; resources, Jung-Sik Kong; data curation, Kyungrok Kwon and Hyok Chu Choi; writing – original draft preparation, Kyungrok Kwon; writing – review and editing, Jung-Sik Kong and Youngjin Choi; visualization, Koochul Ji; supervision, Jung-Sik Kong. All authors have read and agreed to the published version of the manuscript.

Disclosure statement

The authors declare no conflict of interest.

References

ABAQUS. (2020). *ABAQUS user manual*.

American Society of Civil Engineers. (2016). *Minimum design loads and associated criteria for buildings and other structures* (ASCE 7-16).

American Society of Civil Engineers. (2010). *Minimum design loads for buildings and other structures* (ASCE 7-10).

Architectural Institute of Korea. (2016). *Korea building code and commentary*. Seoul, Korea.

ASTM International. (2001). *Standard test method for structural performance of sheet metal roof and siding systems by uniform static air pressure difference* (ASTM E1592).

Azzi, Z., Habte, F., Vutukuru, K. S., Gan Chowdhury, A., & Moravej, M. (2020). Effects of roof geometric details on aerodynamic performance of standing seam metal roofs. *Engineering Structures*, *225*, Article 111303. https://doi.org/10.1016/j.engstruct.2020.111303

Baran, I. (2023). 8 – Reliability analysis of the pultrusion process. In I. Baran (Ed.), *Pultrusion* (2nd ed.) (pp. 195–216). Elsevier. https://doi.org/10.1016/B978-0-32-391613-4.00009-4

Baskaran A., Molleti S., Ko S., & Shoemaker L. (2012). Wind uplift performance of composite metal roof assemblies. *Journal of Architectural Engineering*, *18*(1), 2–15. https://doi.org/10.1061/(ASCE)AE.1943-5568.0000042

Brown, C. B., & Yin, X. (1988). Errors in structural engineering. *Journal of Structural Engineering*, *114*(11), 2575–2593. https://doi.org/10.1061/(ASCE)0733-9445(1988)114:11(2575)

Chauhan, B. S., Chakrabarti, A., & Ahuja, A. K. (2022). Study of wind loads on rectangular plan tall building under interference condition. *Structures*, *43*, 105–130. https://doi.org/10.1016/j.istruc.2022.06.041

Choi, J.-W., Cha, Y., & Kim, J.-Y. (2017). Interdecadal variation of Korea affecting TC activity in early 1980s. *Geoscience Letters*, *4*(1), Article 1. https://doi.org/10.1186/s40562-017-0068-5

Choi, H. C., Ji, K., Kwon, K., & Kong, J. S. (2021). Sustainability of industrial building SSMR through experimental and analytical study under wind uplift load. *Sustainability*, *13*(24), Article 13815. https://doi.org/10.3390/su132413815

Du, X., & Hu, Z. (2012). First order reliability method with truncated random variables. *Journal of Mechanical Design*, *134*(9), Article 091005. https://doi.org/10.1115/1.4007150

Ellingwood, B. R., & Tekie, P. B. (1999). Wind load statistics for probability-based structural design. *Journal of Structural Engineering*, *125*(4), 453–463. https://doi.org/10.1061/(ASCE)0733-9445(1999)125:4(453)

Ellingwood, B. R., Rosowsky, D. V., Li, Y., & Kim, J. H. (2004). Fragility assessment of light-frame wood construction subjected to wind and earthquake hazards. *Journal of Structural Engineering*, *130*(12), 1921–1930. https://doi.org/10.1061/(ASCE)0733-9445(2004)130:12(1921)

Chowdhury, G. A., Zisis, I., Irwin, P., Bitsuamlak, G., Pinelli, J.-P., Hajra, B., & Moravej M. (2017). Large-scale experimentation using the 12-fan wall of wind to assess and mitigate hurricane wind and rain impacts on buildings and infrastructure systems. *Journal of Structural Engineering*, *143*(7), Article 04017053. https://doi.org/10.1061/(ASCE)ST.1943-541X.0001785

Geng, Y., Han, X., Zhang, H., & Shi, L. (2021). Optimization and cost analysis of thickness of vacuum insulation panel for structural insulating panel buildings in cold climates. *Journal of Building Engineering*, *33*, Article 101853. https://doi.org/10.1016/j.jobe.2020.101853

Gill, A., Genikomsou, A. S., & Balomenos, G. P. (2021). Fragility assessment of wood sheathing panels and roof-to-wall connections subjected to wind loading. *Frontiers of Structural and Civil Engineering*, *15*(4), 867–876. https://doi.org/10.1007/s11709-021-0745-5

Hong, H. P., & He, W. X. (2015). Effect of human error on the reliability of roof panel under uplift wind pressure. *Structural Safety*, *52*, 54–65. https://doi.org/10.1016/j.strusafe.2014.07.001

Hoxha, D., Ismail, B., Rotaru, A., Izabel, D., & Renaux, T. (2022). Assessment of the usability of some bio-based insulation materials in double-skin steel envelopes. *Sustainability*, *14*(17), Article 10797. https://doi.org/10.3390/su141710797

Jeong, S.-H., Kim, B.-J., & Ha, Y.-C. (2014). Revision of basic wind speed map of KBC-2009. *Journal of the Architectural Institute of Korea Structure & Construction*, *30*(5), 37–47. https://doi.org/10.5659/JAIK_SC.2014.30.5.037

Ji, K., Choi, H. C., Kwon, K., & Kong, J. S. (2022). Numerical and experimental studies of mechanical performance and structural enhancement of industrial building SSMRs. *Materials*, *15*(9), Article 3163. https://doi.org/10.3390/ma15093163

Kennedy, R. P., & Ravindra, M. K. (1984). Seismic fragilities for nuclear power plant risk studies. *Nuclear Engineering and Design*, *79*(1), 47–68. https://doi.org/10.1016/0029-5493(84)90188-2

Konthesingha, K. M. C., Stewart, M. G., Ryan, P., Ginger, J., & Henderson, D. (2015). Reliability based vulnerability modelling of metal-clad industrial buildings to extreme wind loading for cyclonic regions. *Journal of Wind Engineering and Industrial Aerodynamics*, *147*, 176–185. https://doi.org/10.1016/j.jweia.2015.10.002

Korean Agency for Technology and Standards. (2018). *Hot-dip zinc-coated steel sheets and coil* (KS D 3506). Seoul, Korea.

Lee, K. H., & Rosowsky, D. V. (2005). Fragility assessment for roof sheathing failure in high wind regions. *Engineering Structures*, *27*(6), 857–868. https://doi.org/10.1016/j.engstruct.2004.12.017

Lee, S., Ham, H. J., & Kim, H.-J. (2013). Fragility assessment for cladding of industrial buildings subjected to extreme wind. *Journal of Asian Architecture and Building Engineering*, *12*(1), 65–72. https://doi.org/10.3130/jaabe.12.65

Li, Y., & Stewart, M. G. (2011). Cyclone damage risks caused by enhanced greenhouse conditions and economic viability of strengthened residential construction. *Natural Hazards Review*, *12*(1), 9–18. https://doi.org/10.1061/(ASCE)NH.1527-6996.0000024

Lopez, J. M., Roueche, D. B., & Prevatt, D. O. (2020). Wind resistance and fragility functions for wood-framed wall sheathing panels in low-rise residential construction. *Journal of Structural Engineering*, *146*(8), Article 04020139. https://doi.org/10.1061/(ASCE)ST.1943-541X.0002653

Lu, Q., Li, M., Zhang, M., Min, Q., Zhang, Y., & Liu, X. (2022). Wind-resistance performance investigation of 360° vertical seam-locked roof system reinforced by sliding support and sandwich panel. *Journal of Building Engineering*, *45*, Article 103689. https://doi.org/10.1016/j.jobe.2021.103689

Madsen, H. O., Krenk, S., & Lind, N. C. (2006). *Methods of structural safety*. Courier Corporation.

Maier, H. R., Lence, B. J., Tolson, B. A., & Foschi, R. O. (2001). First-order reliability method for estimating reliability, vulnerability, and resilience. *Water Resources Research*, *37*(3), 779–790. https://doi.org/10.1029/2000WR900329

Masanobu, S., Feng, M. Q., Lee, J., & Naganuma, T. (2000). Statistical analysis of fragility curves. *Journal of Engineering Mechanics*, *126*(12), 1224–1231. https://doi.org/10.1061/(ASCE)0733-9399(2000)126:12(1224)

Matousek, M. (1983). *Measures against errors in the building process* (NASA STI/Recon Technical Report N, 84, 15295). National Research Council of Canada.

Mehta, K. C., Levitan, M. L., Iverson, R. E., & McDonald, J. R. (1992). Roof corner pressures measured in the field on a low building. *Journal of Wind Engineering and Industrial Aerodynamics*, *41*(1), 181–192. https://doi.org/10.1016/0167-6105(92)90408-3

Melchers, R. E., & Beck, A. T. (2018). *Structural reliability analysis and prediction*. John Wiley & Sons. https://doi.org/10.1002/9781119266105

Min, Q., Li, N., Zhang, Y., Lu, Q., & Liu, X. (2021). A novel wind resistance sliding support with large sliding displacement and high tensile strength for metal roof system. *Engineering Structures*, *243*, Article 112670. https://doi.org/10.1016/j.engstruct.2021.112670

Mohammadabadi, M., Yadama, V., & Dolan, J. D. (2021). Evaluation of wood composite sandwich panels as a promising renewable building material. *Materials*, *14*(8), Article 2083. https://doi.org/10.3390/ma14082083

Nowak, A. S., & Collins, K. R. (2012). *Reliability of structures*. CRC press. https://doi.org/10.1201/b12913

Pinelli, J.-P., Simiu, E., Gurley, K., Subramanian, C., Zhang, L., Cope, A., Filliben, J. J., & Hamid, S. (2004). Hurricane damage prediction model for residential structures. *Journal of Structural Engineering*, *130*(11), 1685–1691. https://doi.org/10.1061/(ASCE)0733-9445(2004)130:11(1685)

Sivapathasundaram, M., & Mahendran, M. (2018). Development of suitable strengthening methods for thin steel roof battens subject to pull-through failures. *Journal of Architectural Engineering*, *24*(2), Article 04018004. https://doi.org/10.1061/(ASCE)AE.1943-5568.0000302

Stewart, M. G. (1993). Structural reliability and error control in reinforced concrete design and construction. *Structural Safety*, *12*(4), 277–292. https://doi.org/10.1016/0167-4730(93)90057-8

Stewart, M. G., Ryan, P. C., Henderson, D. J., & Ginger, J. D. (2016). Fragility analysis of roof damage to industrial buildings subject to extreme wind loading in non-cyclonic regions. *Engineering Structures*, *128*, 333–343. https://doi.org/10.1016/j.engstruct.2016.09.053

Straub, D., & Der Kiureghian, A. (2008). Improved seismic fragility modeling from empirical data. *Structural Safety*, *30*(4), 320–336. https://doi.org/10.1016/j.strusafe.2007.05.004

Wang, M., Ou, T., Xin, Z., Wang, D., Zhang, Y., & Cui, L. (2021). Experimental study on static temperature field effect on standing seam metal roof system. *Structures*, *31*, 1–13. https://doi.org/10.1016/j.istruc.2021.01.078

Zhang, H., Hou, S., Ding, Y., Li, C., & Liu, P. (2021). Fragility comprehensive assessment of low-rise cold-formed steel framed wall structure subjected to wind load. *Shock and Vibration*, *2021*, Article 6969967. https://doi.org/10.1155/2021/6969967